Inorganic Chemistry

Article

pubs.acs.org/IC

Synthesis, Crystal Structures, Magnetic, and Thermal Properties of Divalent Metal Formate–Formamide Layered Compounds.

Pradeep Samarasekere, Xiqu Wang, Allan J. Jacobson,* Joshua Tapp, and Angela Möller*

Department of Chemistry and Texas Center for Superconductivity, University of Houston, Houston, Texas 77204-5003, United States

Supporting Information

ABSTRACT: A series of layered divalent metal formate compounds, $[M(HCOO)_2(HCONH_2)_2]$ (M = Mn (1Mn), Ni (2Ni), Cu(3Cu), Zn(4Zn), Mg(5Mg)), have been prepared by solvothermal synthesis and their room temperature (RT) and low-temperature (LT) crystal structures, and thermal and magnetic properties determined. All the compounds contain octahedral metal ions connected by four *anti-anti* formato ligands to form (4,4) nets with the composition of $M(HCOO)_2$. The oxygen atoms from two coordinating formamide ligands above and below the layer complete the MO_6 distorted octahedral coordination. Order–disorder phase transformations involving the formamide ligands were observed in the 1Mn, 2Ni, and 4Zn compounds. Like transitions in related formate structures with perovskite like topology, the transitions correspond to the ordering of the amine groups of the terminating formamide ligands which are disordered at ambient temperature. The magnetic properties of the three magnetic members of the series 1Mn, 2Ni, and 3Cu were investigated using microcrystalline samples, over the temperature range of 2 K–300 K under different applied fields. All compounds belong to antiferromagnetic square lattices with S = 5/2, 1, and 1/2. Exchange constants for a nearest neighbor model are presented here. Specific heat measurements indicate magnetic long-range order at lower temperatures, S = 5/2 (antiferromagnetic) and S = 1 (ferrimagnetic).

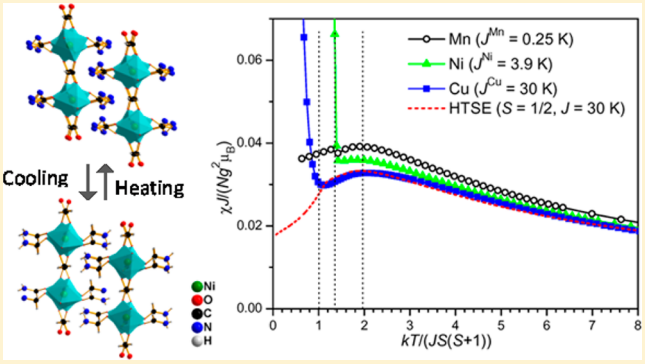

INTRODUCTION

Metal–organic frameworks (MOFs) or more generally coordination polymers[1] are inorganic–organic hybrid materials which are made up of metal cations assembled into extended structures by coordinating with organic bridging ligands. Research in this field has grown over the past two decades, in part because of the high porosity and high surface area shown by many MOFs[2] which leads to potential applications in selective adsorption and separation of gas molecules[3] and in catalysis.[4] Moreover, the large number of ligands and metals that can be used in assembling MOFs enables the introduction of other physical properties such as conductivity,[5] optical behavior,[6] and magnetism,[7] leading to possible applications in other areas.[8]

Magnetic MOFs have attracted some attention and show some interesting and unusual magnetic phenomena.[7,8a] The structural and chemical flexibility of the diamagnetic ligands used to connect magnetic d or f metal ions into extended networks enables the design and assembly of magnetic MOFs with low-dimensional features, such as chains,[9] or layers,[10] as well as three-dimensional frameworks.[11] The 3d transition metals provide variations of magnetic anisotropy and spin quantum numbers,[7a] and many studies have been reported in the recent literature. It remains of interest to synthesize and study iso-structural or iso-topological series of transition MOFs containing different 3d metals to investigate structure–property correlations.

The magnetic properties of a MOF depend on the magnetic coupling between the paramagnetic metal centers. The magnetic exchange between transition metal centers usually takes place via a cation-ligand-cation superexchange pathway,[12] which strongly depends on the relative orientation of the orbitals and the distance between the interacting metal centers. The diamagnetic organic linkers provide an efficient magnetic exchange pathway by establishing an overlap between metal and ligand orbitals that lowers the total energy. With this in mind, many different types of short bridging ligands including halide (X^-), bifluoride (HF_2^-), cyanide (CN^-), azide (N_3^-), cyanate (OCN^-), thiocyanate (SCN^-), dicyanamide ($N(CN)_2^-$), and formate ($HCOO^-$) have been used to build magnetic MOFs.[13]

Formate, the smallest carboxylic ligand, was studied several decades ago because of the unusual physical properties observed in hydrated transition metal formate compounds.[14,15] A renewed interest in formate based frameworks has occurred recently.[16] The formate ligand adopts different bridging modes depending on the coordination environment.[16a] In an environ-

Received: August 28, 2013
Published: December 12, 2013

   dx.doi.org/10.1021/ic402200v | Inorg. Chem. 2014, 53, 244–256

ment with no bulky ligands, formate favors the μ-HCO_2^--*anti-anti* bridging mode for metal coordination.[17] This coordination mode promotes an effective superexchange coupling between metal ions. The origin of the coupling can be described as a consequence of delocalization of the electrons in the formate anion represented by the resonance hybrid structures (—O═C(H)—O— and —O−C(H)═O—).[18] Thus it behaves like a diamagnetic single atom but, in an excited state, can transfer π-electrons to one of the connected metal ions. As a consequence, the formate anion acquires a magnetic moment induced by the spin of the metal ion enabling the adjacent metal ions to interact. Thus, the neighboring metal centers are effectively coupled via the formate bridging ligand leading to interesting magnetic behavior. The structure−property relationship of hydrated transition metal formates $M(HCOO)_2{\cdot}xH_2O$ (M = transition metals) and their deuterated forms,[14,15,19] anhydrous metal formates $[M(HCOO)_2]$,[20] metal formates with monodentate ligands $[M(HCOO)_2{\cdot}2L]$ (L = urea),[21] metal formates with bidentate ligands $[M(HCOO)_2L]$ (L = 4,4′-bipyridine, pyrazine),[22] and metal formates with solvents $[M(HCOO)_2{\cdot}n(\text{solvent})]$[23] have been studied. In many of these compounds the behavior of the magnetic susceptibility below the Néel temperatures suggested weak ferrimagnetism.

Cheetham and co-workers recently demonstrated that both magnetic and antiferroelectric order occurred in a series of formate based transition metal compounds $[(CH_3)_2NH_2][M(HCOO)_3]$.[24] Multiferroic behavior is a relative rare phenomenon given that electric and magnetic behavior tend to be mutually exclusive.[25] Subsequently, multiferroic behavior was found in the series $[NH_4][M(HCOO)_3]$,[26] and $[C(NH_2)_3][Cu(HCOO)_3]$ was suggested as a possible multiferroic material.[27] Several other formate based divalent metal compounds were reported recently as magnetic or ferroic materials.[17,28,29]

In the multiferroic formates with structures related to the ABX_3 perovskite, the organic cation and the formate anion correspond to A and X, respectively. In the room temperature (RT) structures the alkyl ammonium cation at the A site is disordered. At lower temperatures, an order−disorder phase transition occurs giving a dielectric anomaly at the transition temperature. The ordering of ammonium cation is associated with a hydrogen bond ordering which triggers the antiferroelectric ordering in the LT phase. The mechanism for ordering of electric dipoles via hydrogen bond ordering is well documented in literature.[30]

The same effect was observed in layered copper formate tetrahydrate where an antiferroelectric phase transition and an antiferromagnetic transition were observed at LTs.[15] Similar to the perovskite-like formates, the origin of the dielectric anomaly of this compound is also related to an order−disorder transition. The RT structure of $Cu(HCOO)_2{\cdot}4H_2O$ consists of alternating layers of $Cu(HCOO)_2$ and disordered H_2O molecule layers. At the phase transition, the disordered H_2O molecules become ordered triggering a dielectric anomaly. To our knowledge, this type of structural order−disorder transformation has not been observed in any other layered transition metal formate.

In the present work, we report a series of layered divalent metal formates, $[M(HCOO)_2(HCONH_2)_2]$ (M = Mn (**1Mn**), Ni (**2Ni**), Cu(**3Cu**), Zn(**4Zn**), Mg(**5Mg**)), their RT and low-temperature (LT) crystal structures, and their thermal and magnetic properties. All the compounds contain octahedral metal ions connected by four *anti-anti* formato ligands to form (4,4) nets with the composition of $M(HCOO)_2$. The oxygen atoms from two coordinating formamide ligands above and below the layer complete the MO_6 distorted octahedral coordination. Order−disorder phase transformations involving the formamide ligands were observed in the **1Mn**, **2Ni**, and **4Zn** compounds. Like the transitions in the perovskite related formate structures, the transitions are associated with the ordering of the amine groups of the terminating formamide ligands which are disordered at ambient temperature. Only very few formate compounds with formamide as a coligand are known.[31] Among them, $Co(HCOO)_2(HCONH_2)_2$ reported by Rettig et.al.[31a] is also disordered, but no reference to an order−disorder transformation is given. The magnetic properties of the three magnetic members of the series **1Mn**, **2Ni**, and **3Cu** were investigated using microcrystalline samples, over the temperature range of 2 K−300 K under different applied fields. The overall behavior of the compounds corresponds to an effective antiferromagnetic (AF) exchange of adjacent magnetic centers on the square lattice. At LTs, **1Mn** and **2Ni** exhibit long-range order (LRO) of the antiferro- and ferrimagnetic type, respectively. For the **3Cu** no LRO could be detected by specific heat measurements down to 2 K.

EXPERIMENTAL SECTION

Materials. All starting materials were reagent grade, commercially available (Sigma-Aldrich; U.S.), and were used without further purification.

Synthesis of 1Mn. $Mn(HCOO)_2{\cdot}(HCONH_2)_2$ was obtained by reacting $MnCl_2{\cdot}4H_2O$ (0.198 g, 1 mmol) with 10 mL of formamide in a 22 mL sealed vial, heated to 90 °C under autogenous pressure for 96 h. Square pyramidal-shaped colorless crystals were obtained with a yield of 65% based on Mn. The product was vacuum-dried. Anal. Calcd. for $MnH_8C_4N_2O_6$ (%); C, 20.44; N, 11.92; H, 3.43. Found; C, 20.59; N, 11.82; H, 3.71.

Synthesis of 2Ni. $Ni(HCOO)_2{\cdot}(HCONH_2)_2$ was obtained by reacting $NiCl_2{\cdot}6H_2O$ (0.238 g, 1 mmol) with 10 mL of formamide in a 22 mL sealed vial, heated to 70 °C under autogenous pressure for 48 h. Square pyramidal shaped green crystals were obtained in a yield of 80% based on Ni. The product was vacuum-dried. Anal. Calcd. for $NiH_8C_4N_2O_6$ (%); C, 20.12; N, 11.73; H, 3.38. Found; C, 20.31; N, 11.76; H, 3.67.

Synthesis of 3Cu. $Cu(HCOO)_2{\cdot}(HCONH_2)_2$ was obtained by reacting $CuCl_2{\cdot}2H_2O$ (0.170 g, 1 mmol) with 10 mL of formamide in a 22 mL sealed vial, heated to 70 °C under autogenous pressure for 72 h. The resulted clear blue solution was cooled to RT at ambient atmosphere and kept undisturbed in the sealed vial. Square bipyramidal shaped blue crystals were obtained in a yield of 60% based on Cu after 3 weeks. The product was vacuum-dried. Anal. Calcd. for $CuH_8C_4N_2O_6$ (%); C, 19.72; N, 11.5; H, 3.31. Found; C, 19.96; N, 11.46; H, 3.59.

Synthesis of 4Zn. $Zn(HCOO)_2{\cdot}(HCONH_2)_2$ was obtained by reacting $Zn(NO_3)_2{\cdot}6H_2O$ (0.297 g, 1 mmol) with 10 mL of formamide in a 22 mL sealed vial, heated to 90 °C under autogenous pressure for 96 h. The resulted clear colorless solution was cooled to RT at ambient atmosphere and kept undisturbed in the sealed vial. Square pyramidal shaped colorless crystals were harvested in a yield of 40% based on Zn after about 2 months. The product was vacuum-dried. Anal. Calcd. for $ZnH_8C_4N_2O_6$ (%); C, 19.70; N, 11.48; H, 3.28. Found; C, 19.68; N, 10.98; H, 3.32.

Synthesis of 5Mg. $Mg(HCOO)_2{\cdot}(HCONH_2)_2$ was obtained by reacting $MgCl_2$ (0.095 g, 1 mmol, 1.5% H_2O) with 10 mL of formamide. The reaction mixture was stirred for 1 h in air and transferred to a 22 mL vial. The sealed vial was heated to 100 °C under autogenous pressure for 96 h. The resulted clear colorless solution was cooled to RT at ambient atmosphere and kept undisturbed in the sealed vial. Square pyramidal shaped colorless crystals were harvested in a yield of 65% based on Mg after 3 weeks. The product was dried

dx.doi.org/10.1021/ic402200v | *Inorg. Chem.* 2014, 53, 244−256

Table 1. Crystal Data for All Compounds

	1Mn	1bMn	1cMn	2Ni	2bNi	3Cu	4Zn	4bZn	5Mg
formula	$C_4H_8MnN_2O_6$	$C_4H_8MnN_2O_6$	$C_4H_8MnN_2O_6$	$C_4H_8NiN_2O_6$	$C_4H_8NiN_2O_6$	$C_4H_8CuN_2O_6$	$C_4H_8ZnN_2O_6$	$C_4H_8ZnN_2O_6$	$C_4H_8MgN_2O_6$
formula wt.	235.06	235.06	235.06	238.83	238.83	243.66	245.49	245.49	204.43
T (K)	298	203	153	298	233	298	298	163	298
crys. system	monoclinic	monoclinic	monoclinic	monoclinic	monoclinic	monoclinic	monoclinic	monoclinic	monoclinic
S.G.	$C2/c$	$C2/c$	$C2/c$	$C2/c$	$P2_1/c$	$P2_1/c$	$C2/c$	$P2_1/c$	$P2_1/c$
a (Å)	12.731(2)	12.536(6)	25.039(2)	12.764(2)	7.361(2)	7.780(1)	12.808(2)	7.446(2)	8.6278(9)
b (Å)	8.552(1)	8.623(5)	34.572(3)	8.246(1)	8.088(2)	7.953(1)	8.314(1)	8.109(2)	8.4343(9)
c (Å)	8.511(1)	8.341(4)	8.2874(8)	8.190(1)	8.295(2)	8.006(1)	8.268(1)	8.339(2)	12.153(1)
α (deg)	90.00	90.00	90.00	90.00	90.00	90.00	90.00	90.00	90.00
β (deg)	93.558(2)	95.884(3)	96.231(1)	92.646(2)	116.82(2)	115.115(2)	93.065(2)	117.06(2)	91.033(1)
γ (deg)	90.00	90.00	90.00	90.00	90.00	90.00	90.00	90.00	90.00
V (Å^3)	924.8(2)	896.9(9)	7131.7(1)	861.1(2)	440.7(2)	448.5(1)	879.1(2)	448.4(2)	884.2(2)
Z	4	4	32	4	2	2	4	2	4
D_{cal}	1. 688	1.741	1.751	1.842	1.800	1.804	1.855	1.818	1.536
F000	476	476	3808	488	244	246	496	248	424
μ (mm^{-1})	1.43	1.474	1.483	2.255	2.203	2.437	2.796	2.741	0.204
Θ_{min}, Θ_{max} (deg)	2.87, 28.47	2.87, 27.45	1.18, 28.31	2.94, 28.35	3.73, 27.81	2.89, 28.33	2.92, 28.34	3.95, 28.12	2.36, 28.33
no. of tot. ref.	2700	2968	24965	2476	973	2620	2591	1126	5855
unique ref.	1076	995	8383	992	916	1052	1023	1017	2076
R(int)	0.0360	0.0539	0.0747	0.0225	0.0297	0.0698	0.0874	0.0254	0.0355
no. of obs. [$I > 2\sigma(I)$]	1020	980	3646	936	735	830	963	922	1921
paramet/restrains	83/1	72/0	524/0	75/0	69/1	61/0	74/11	61/0	153/0
R1, wR2 [$I > 2\sigma(I)$]	0.0324, 0.0871	0.0321, 0.0936	0.0492, 0.1734	0.0294, 0.0758	0.0326, 0.0892	0.0340, 0.0878	0.0423, 0.1208	0.0242, 0.0734	0.0308, 0.0903
R1, wR2 [all data]	0.0338, 0.0886	0.0325, 0.0939	0.0862, 0.2034	0.0304, 0.0767	0.0454, 0.0921	0.0439, 0.0921	0.0433, 0.1221	0.0266, 0.0745	0.0330, 0.0915
GOF	1.061	1.333	1.102	1.064	1.160	0.961	1.159	1.259	1.047
largest diff. peak and hole (e/Å^3)	0.36, −0.57	0.73, −0.22	1.12, −0.72	0.58, −0.63	0.73, −0.51	0.50, −0.67	0.92, −1.16	0.96, −0.50	0.23, −0.36

dx.doi.org/10.1021/ic402200v | Inorg. Chem. 2014, 53, 244−256

under vacuum. Anal. Calcd. for $MgH_8C_4N_2O_6$ (%); C, 23.48; N, 13.70; H, 3.94. Found; C, 22.96; N, 13.36; H, 3.99.

Crystal Structure Determination. Single crystal data were collected using a Siemens SMART platform diffractometer equipped with an APEX2 area detector and using monochromatic Mo Kα radiation (λ = 0.71073 Å). A single crystal of suitable size was selected, coated with paraffin oil to prevent deterioration in humid air, and mounted on a glass fiber using silicone glue for each phase. Crystals used for LT data collections were protected by epoxy instant glue to limit the effects of crystal cracking at phase transitions. This turned out to be a simple but necessary precaution as the hardened glue prevented the movements of cracked crystal domains. Data sets were collected at 298 K for **1Mn**, **2Ni**, **3Cu**, **4Zn**, and **5Mg**, at 213 K for **1bMn**, at 153 K for **1cMn**, at 233 K for **2bNi**, and at 163 K for **4bZn**. A N_2 cold stream was used to maintain the LTs. Data collection, cell refinement, data integration and reduction were performed by using the APEX2 system.[32] The structures were solved by direct methods using the SHELXS97[33] program and refined by using the SHELXL97[34] program, both integrated in the WinGX[35] package. The crystals of the Ni and Zn compounds were twinned at LTs, and the data were deconvoluted using CELL_NOW.[36] Two domains were found for both Ni and Zn crystals with twinning ratios of 0.82 and 0.80 respectively. No twinning was observed for samples of 1bMn and 1cMn. Weak superstructure reflections of 1cMn were observed, and the structure was refined with the superstructure unit cell 8-fold larger than that of 1aMn. The hydrogen atoms of the formate ions were found in the Fourier maps and refined isotropically. The hydrogen atoms of the formamide were added at the best geometric positions, and refined with geometrical constraints. The hydrogen atoms of the NH_2 groups of Mn, Ni, and Zn compounds could not be found in Fourier maps and were not added because of the high degree of disorder of the formamide ligands. Crystal data are summarized in Table 1. A summary of the four distinct polymorphs is provided in Table 2

Table 2. Summary of the Observed Structure Types for the $[M(HCOO)_2(HCONH_2)_2]$ Series of Compounds

compound	polymorph	space group	disorder
1Mn	I	$C2/c$	3 inequivalent N positions
1bMn	I	$C2/c$	2 inequivalent N positions
2Ni	I	$C2/c$	2 inequivalent N positions
4Zn	I	$C2/c$	5 inequivalent N positions
3Cu	II	$P2_1/c$	ordered
2bNi	II	$P2_1/c$	ordered
4bZn	II	$P2_1/c$	ordered
5Mg	III	$P2_1/c$	ordered, 2 inequivalent Mg
1cMn	IV	$C2/c$	disordered and ordered formamides, 4 inequivalent Mn

The purities of the phases were confirmed by powder X-ray diffraction at RT with a PANalytical X'pert PRO diffractometer. Data were collected using Cu Kα radiation (λ = 1.54187 Å), over the range of $5° < 2\theta < 90°$ and compared with theoretical patterns simulated from the respective single crystal data (Supporting Information, Figure S1).

Characterization. Infrared spectra of the samples were measured with a Galaxy series FTIR 5000 spectrometer using KBr pellets in the range 400 to 4000 cm^{-1} at ambient conditions. Elemental analyses were performed by Galbraith Laboratories (Knoxville, TN).

Physical Property Measurements. The magnetic properties of the compounds were measured using a Quantum Design Physical Property measurement System (QD-PPMS) equipped with a vibrating-sample magnetometer. Microcrystalline powders were used in the analyses. Measurements were made in both zero-field cooled (ZFC) and field cooled (FC) conditions at fields from 500 Oe to 5 T. Diamagnetic corrections were estimated using Pascal constants[37] (-115×10^{-6} emu/mol for **1Mn**, -113×10^{-6} emu/mol for **2Ni**, and -112×10^{-6} emu/mol for **3Cu**).

Heat capacity measurements were performed at fields up to 5 T on the same QD-PPMS system with microcrystalline powders pressed into pellets.

DSC measurements were performed on a Mettler Toledo gas controller DSC system. Microcrystalline samples were placed in an aluminum crucible and heated up to 323 K and then cooled down to 123 K at a rate of 20 K min^{-1} under nitrogen and cycled twice. Isothermal equilibrations for 5 min were used between cooling and heating.

Thermogravimetric analyses were performed using Hi-Res TGA 2950 thermogravimetric system. Samples were heated in air to 323 K and isothermally equilibrated at that temperature for 30 min followed by heating to 623 K for **1Mn**−**4Zn** and to 773 K for **5Mg** with a heating rate at 1 °C min^{-1}.

RESULTS AND DISCUSSION

Synthesis. All the compounds were prepared by the reaction of divalent metal cations with formamide under mild solvothermal conditions at 70−100 °C. The reaction temperature and time were systematically varied to obtain the optimum conditions for each reaction. Pure crystalline phases of each compound were obtained. The phase purity was confirmed by comparison of the powder X-ray patterns with patterns simulated from the single crystal X-ray data (Supporting Information, Figure S1).

Formamide plays an important role in this synthesis. It behaves both as the source of formate and formamide and serves as the solvent for the crystallization. At an elevated temperature and pressure formamide is hydrolyzed to form formate.[38a] The reaction kinetics and the mechanism of this hydrolysis have been widely investigated both experimentally and theoretically, and several mechanisms have been proposed.[38] In our experiments, the lattice water in the starting metal salts provides the source of water for the formation of the formate anion.

Crystal Structures. Single-crystal X-ray structure data of **1Mn**−**5Mg** at RT (298 K) revealed that **1Mn**, **1bMn**, **2Ni**, **4Zn** are isostructural (structure type I) and crystallize in the monoclinic space group $C2/c$ with small differences in lattice parameters. These compounds have the same structure as $Co(HCOO)_2{\cdot}(HCONH_2)_2$ reported by Rettig et al.[31a] The compounds **3Cu**, **2bNi** at (233 K) and **4bZn** (163K) are isostructural in the monoclinic space group $P2_1/c$ (structure type II). The **5Mg** compound (type III) crystallizes in the monoclinic space group $P2_1/c$ and has two inequivalent Mg atoms. The cell dimensions are similar to (I) if a and c axes are interchanged. The 1cMn structure (type IV) has the same space group as (I), but has a 8-fold larger unit cell with doubled a and quadrupled b cell dimensions compared to (I). The LT **1cMn** structure (type (IV)) is an isomorphic subgroup of structure type (I) with a subgroup index 8. The **3Mg** structure (type (III)) may be considered as a k2 ("klassengleich" with index 2) subgroup of (I). Structure type (II) is not a subgroup of (I), because the loss of C-centering translation symmetry is replaced by translation symmetry of halving cell volume. The phase transition between (I) and (II) probably involves intermediate subgroups common to both structures. The different structure types are summarized in Table 2. Selected bond distances and bond angles are listed in Supporting Information, Table S1.

Room Temperature Structures. *Structures of 1Mn, 2Ni, and 4Zn.* The structures of compounds **1Mn**, **2Ni**, and **4Zn**

dx.doi.org/10.1021/ic402200v | Inorg. Chem. 2014, 53, 244−256

contain one crystallographically independent divalent metal ion (Figure 1a). The metal ion in each structure is located on the 2-fold axis. All the metal ions are six coordinated by oxygen atoms in a nearly regular octahedral coordination environment. The equatorial positions of the octahedron are occupied by four oxygen atoms from four different bridging formates in an *anti-anti* arrangement. The axial sites are occupied by two oxygen atoms from two nonbridging formamide molecules. Each octahedron is linked to four neighboring metal ions through four bridging formate ligands to form a two-dimensional infinite layer with the composition $M(HCOO)_2$ (Figure 1b). The areas of the squares defined by four nearest neighbor metal atoms are 36.392(5) Å^2 for **1Mn**, 33.769(5) Å^2 for **2Ni**, and 34.368(5) Å^2 for **4Zn**.

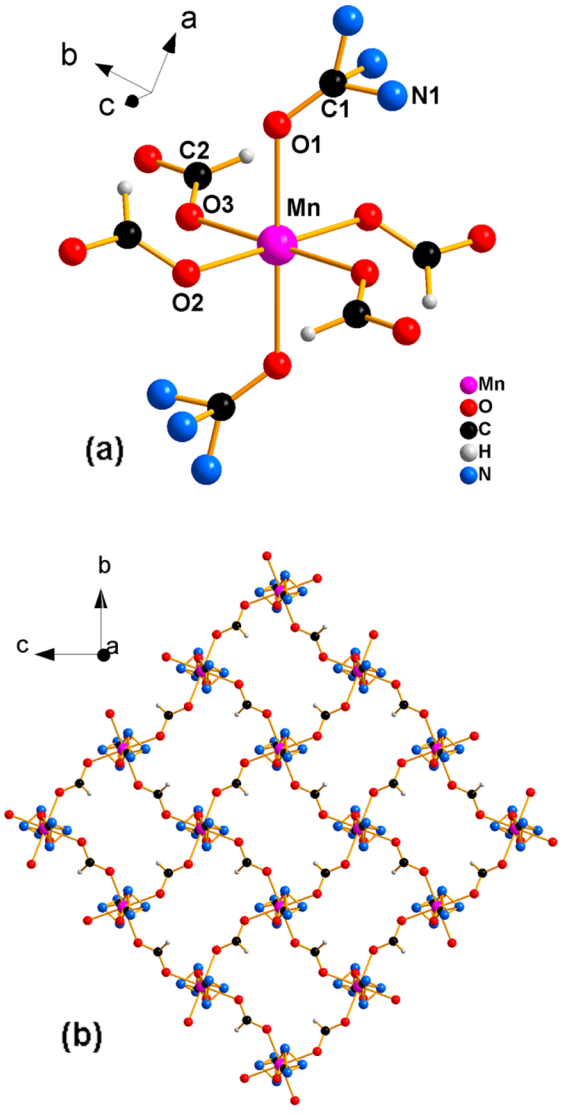

Figure 1. (a) Local coordination environment of Mn with atom labeled. (b) View of 2D (4,4) network of **1Mn** in *bc* plane.

The O−C−O angle of the formate ligand gives rise to a characteristic tilting of the MO_6 octahedra. Neighboring octahedra are tilted relative to one another with dihedral angles of 27.21(6)° for **1Mn**, 27.80(6)° for **2Ni**, and 27.3(1)° for **4Zn**. All the MO_6 octahedra are distorted with four short equatorial bonds 2.163(1), 2.164(2) Å for **1Mn**, 2.048(1), 2.054(1) Å for **2Ni**, and 2.077(2) Å, 2.087(2) Å for **4Zn**) and two long apical bonds (2.198(1) Å for **1Mn**, 2.079(2) Å for **2Ni**, and 2.136(2) Å for **4Zn**). These distances are comparable to those previously reported for other series of metal formates.[19−24]

Analysis of the single crystal X-ray data from **1Mn**, **2Ni**, and **4Zn** indicates that the nitrogen atom of the terminal formamide group is disordered. In **1Mn**, the disorder of nitrogen atom was modeled by including three nonequivalent positions with occupancies of 0.603(4), 0.265(9), and 0.132(9) in the refinement. In **2Ni** the disordering of nitrogen atom was modeled with two positions with occupancies of 0.840(8) and 0.160(8). In **4Zn** five nonequivalent nitrogen positions were refined with the relative occupancies of 0.27(1), 0.265(4), 0.23(1), 0.145(7), and 0.08(1).

The (4,4) infinite layers lie parallel to the crystallographic *bc* plane in **1Mn**, **2Ni**, and **4Zn**. The layers are stacked along the *a* axis and separated by *a*/2 with a shift of *b*/2 along the *b* axis relative to the adjacent layer (Figure 2a). The formamide groups attached to the axial sites of the metals are arranged as spacers between the stacked layers. Only one type of formamide orientation is observed for **1Mn**, **2Ni**, and **4Zn**.

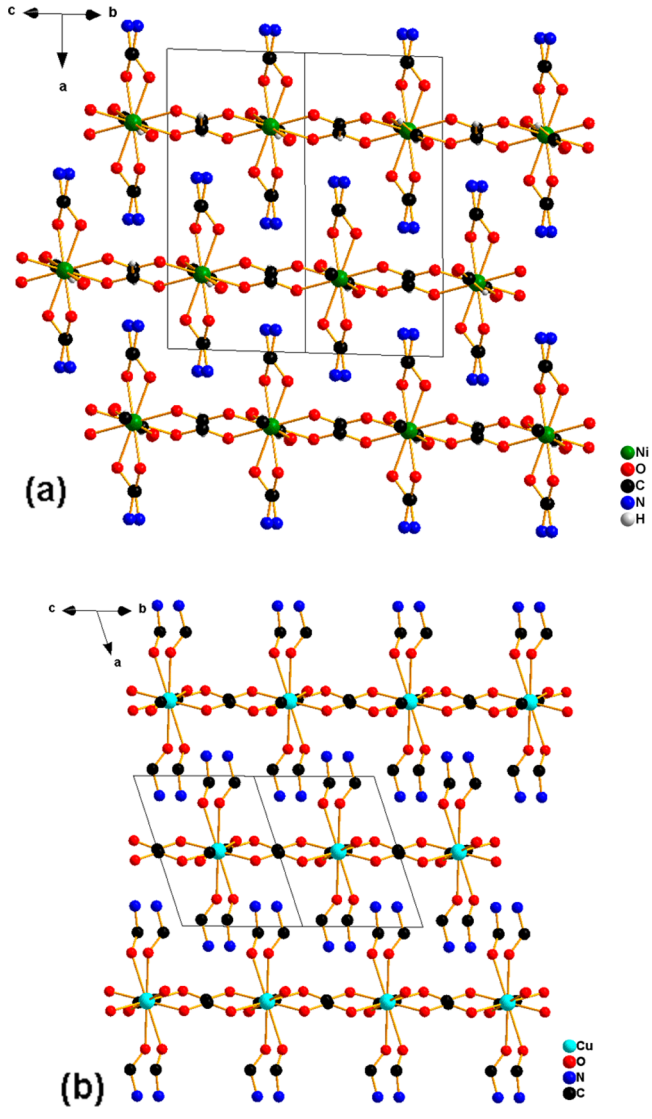

Figure 2. Layer stacking of (a) **2Ni**, (b) **3Cu**. Hydrogen and the disordered nitrogen atoms are omitted for clarity.

dx.doi.org/10.1021/ic402200v | *Inorg. Chem.* 2014, 53, 244−256

The NH_2 groups between adjacent layers form weak N−H···O hydrogen-bonds with bridging formate groups (average N···O distance of 2.96 Å for **1Mn**, 2.99 Å for **2Ni**, and 2.94 Å for **4Zn**). Even though all these hydrogen bonds are weak, they play an important role in connecting the adjacent metal−formate layers together.

*Structure of **3Cu**.* The **3Cu** compound has a similar metal ion coordination environment to the other members of the family. Unlike in **1Mn**, **2Ni**, and **3Zn**, the terminating formamide ligand is ordered in **3Cu** crystallizing in the space group $P2_1/c$. The Cu compound was first observed by Chulkevich et al.[39] as a minor product but has not been fully characterized.

In **3Cu**, one crystallographically independent Cu^{2+} ion is observed to display a Jahn−Teller distortion with four short equatorial bond lengths of 1.963(2), 1.977(2) Å and two long apical ones of 2.370(2) Å. The Cu−O distances are comparable to those observed in other metal-formate frameworks. The bond angles of **3Cu** are in the same range as of the other members of the family. The tilt angle of 19.35(9)° between the neighboring CuO_6 octahedra, however, is slightly smaller than found for the other members.

The $Cu(HCOO)_2$ layers in **3Cu**, as observed also in **1Mn**, **2Ni**, and **4Zn**, lie parallel to the *bc* plane and are stacked along *a* axis (Figure 2b). The layer separation is larger because of the long axial Cu−O bonds of the distorted CuO_6 octahedra. The layer separation is approximately 7.78 Å. The layers are not shifted relative to each other along either *b* or *c* axes. This geometry facilitates H-bond formation between adjacent formamide groups. They form two nearly linear, weak N−H···O hydrogen bonds of 3.03 Å. Thus one formamide group has two interformamide hydrogen bonds and one formamide−formate hydrogen bond of 2.97 Å. As a result the terminating NH_2 groups of formamides are well ordered.

*Structure of **5Mg**.* The Mg member, **5Mg**, has a different structure to the other members of the family with two crystallographically independent Mg^{2+} ions in space group $P2_1/c$ (Figure 3a). The coordination environment of the Mg ions and the bonding modes of the formate and formamide ligands are similar to the other members of the family. The difference between the two Mg ions arises from two different orientations of the attached formamide groups which are oriented *cis* and *trans* relative to the formate plane. The trans oriented formamide is connected to Mg(1) with a Mg(1)−O−C−N dihedral angle of 176.2(1)° and cis oriented formamide is connected to Mg(2) with a Mg(2)−O−C−N dihedral angle of 14.4(2)°. The MgO_6 octahedra are slightly distorted with bond lengths for Mg(1)−O equal to 2.0447(7), 2.0821(8), and 2.0882(8) Å and for Mg(2) equal to 2.0403(8), 2.08541(7), and 2.0976(8) Å. Two different tilt angles of the MgO_6 octahedra are observed between the neighboring Mg^{2+} ions. The MgO_6 polyhedra are tilted toward the *ab* plane along the diagonal of the $Mg(HCOO)_2$ squares. The $Mg(1)O_6$ and the $Mg(2)O_6$ polyhedra tilt toward to the *ab* plane with tilt angles of 16.20(3) and 16.11(2). The tilt angle between the two Mg polyhedron is 30.69(3)°.

The structure of **5Mg** is related to the structures of the other members of the family. The $Mg(HCOO)_2$ layers of **5Mg** lie parallel to the *ab* plane. The layers are stacked along *c* axis and separated by *c*/2 (Figure 3b). Similar to the **3Cu** compound, the Mg member possesses a well ordered structure. No disorder was observed in the positions of the terminal NH_2 groups. Compared to other members of the family, **5Mg** forms the strongest N−H···O hydrogen-bonds between the terminating formamide and bridging formates with a N···O distance of 2.92 Å.

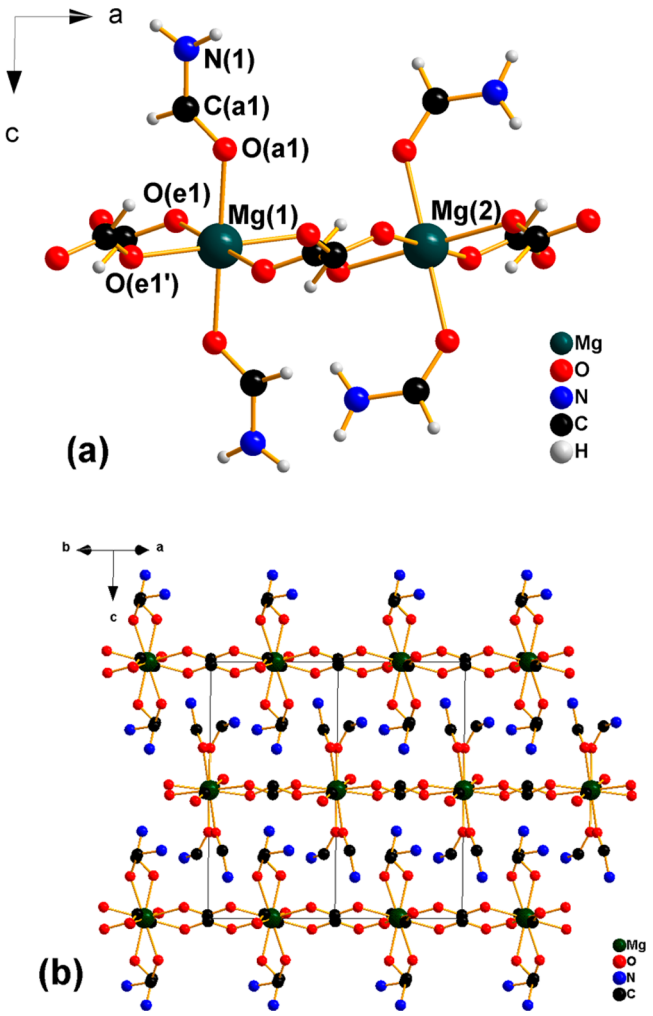

Figure 3. (a) Local coordination environment of Mg with atom labeled and (b) Layer stacking.

Low Temperature Structures. The disorder observed at RT suggested the possibility of order−disorder phase transitions at LT. Despite the fact that several $M(HCOO)_2$ layer type compounds have been reported previously, structural order−disorder phase transformations have been rarely observed in this class of compounds.

The presence of order−disorder transitions in the disordered phases **1Mn**, **2Ni**, and **4Zn** was investigated by differential scanning calorimetry (DSC) (see below) and by LT single crystal X-ray diffraction experiments. The temperatures chosen for the X-ray measurements were based on the DSC results.

*Low Temperature Structures of **1Mn**.* Two phases were observed for the **1Mn** compound at 213 K and at 153 K. Both LT structures have the space group $C2/c$.

The **1bMn** phase at 213 K differs slightly from the RT phase. As a consequence of lowering the temperature, all the cell edges are contracted slightly (Table 1) compared to **1Mn**, the angle β increases, and the volume decreases by 3%. The main difference from the **1Mn** structure was the increase in the degree of order of the formamide NH_2 group. The 3-fold disordered N atom in **1Mn** becomes 2-fold disordered in **1bMn** with almost equal

dx.doi.org/10.1021/ic402200v | Inorg. Chem. 2014, 53, 244−256

occupancies (0.493(7), 0.507(7)). The layer stacking and the extended structure are unaffected by this structural change.

A second phase transition is observed on further lowering the temperature. The structure of this new phase **1cMn** was successfully determined at 153K. The structure of **1cMn** has a larger unit cell compared to the structure of **1Mn**. The cell is expanded by 2 × *a* axis and 4 × *b* axis but no change is observed along the *c* axis; β increases to 96.231(1)°. In contrast to **1Mn** and **1bMn**, the structure of **1cMn** has four crystallographically independent Mn atoms which correspond to different orientations and different degrees of order of the terminating formamide groups. An increase in degree of order of the formamide is observed in the second phase transformation. The two formamide groups coordinated to Mn(1) and Mn(4) (Figure 4a) go from 2-fold disordered to ordered

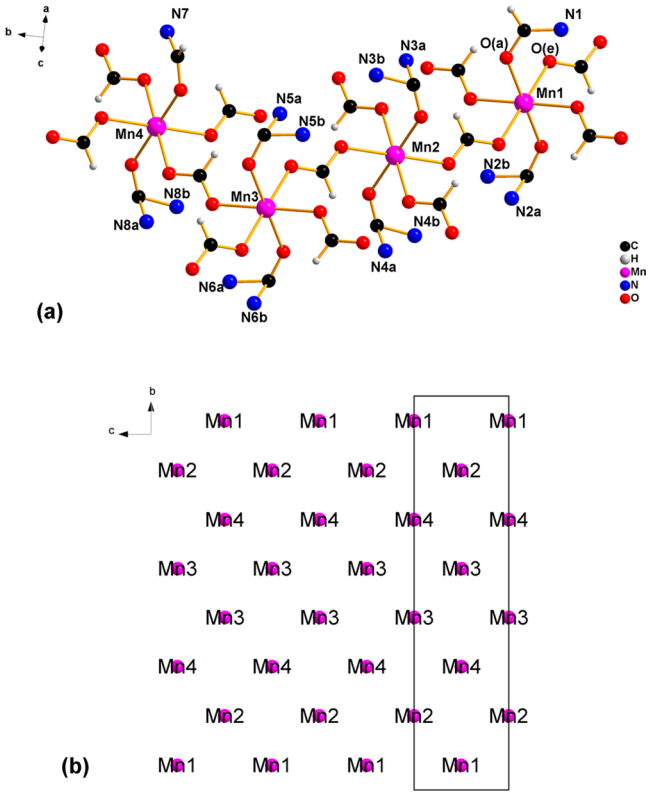

Figure 4. (a) Increase in degree of order and (b) the arrangement of the four in-equivalent Mn ions with in each layer in LT **1cMn**.

while the formamide groups coordinated to Mn(2) and Mn (3) remain 2-fold disordered. The arrangement of the four inequivalent Mn ions within each layer is shown in Figure 4b.

*Low Temperature Structures of **2Ni** and **4Zn**.* Structures were determined at LT for **2Ni** (**2bNi** at 233 K) and **4Zn**, (**4bZn** at 163 K). Both compounds (**2bNi** and **4bZn**) are isostructural with the RT **3Cu** structure, space group $P2_1/c$ with small differences in cell parameters (Table 1). A contraction of the apical M−O bond lengths of the MO_6 octahedra relative to the RT values is observed in both compounds. Two equatorial M—O bonds are expanded, and the other two were contracted in both. The formamide ligands which are disordered in the RT structures are well ordered at LT.

The extended structures of **2bNi** and **4bZn** have a different (4,4) layer stacking arrangement compared to the RT structures. At LT, the (4,4) sheets lie in the $(a-c)b$ plane. Layers are stacked along the [101] direction. In contrast to the RT structures, no layer shift is observed in these LT structures. Weak interformamide hydrogen bonds similar to those observed in **3Cu** are present at LTs (Figure 5).

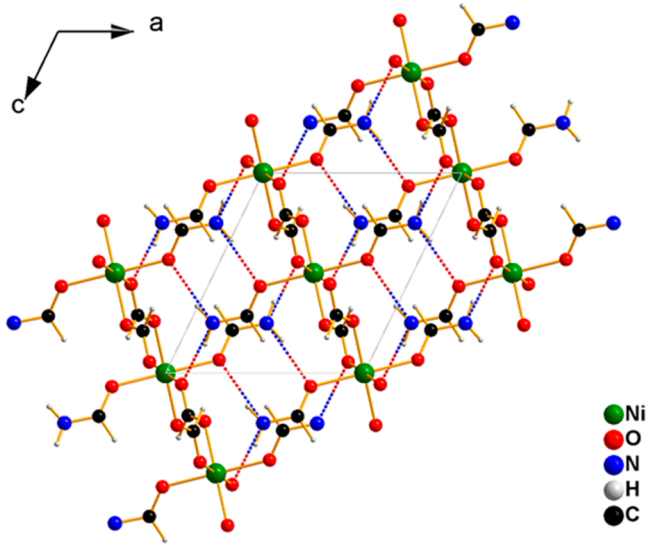

Figure 5. Structure of LT **2bNi** with weak N−H···O bonds.

The NH_2 groups extend into the interlayer space and are only weakly hydrogen bonded to formate oxygen atoms in the adjacent layers. At higher temperatures, the thermal energy is large compared with the strength of the weak formamide-formate hydrogen bonds and disorder results. Lowering the temperature decreases the thermal energy, and a transition eventually occurs where the formamide ligands become ordered.

Differential Scanning Calorimetry (DSC). The thermal behaviors of the compounds at LTs (Figure 6) were determined by DSC measurements. **1Mn**, **2Ni**, and **4Zn** were chosen for DSC measurements because their structures are disordered at RT. Structural phase transitions were observed in the DSC data for each compound. The structural phase transformations are reversible and first order. Upon cooling,

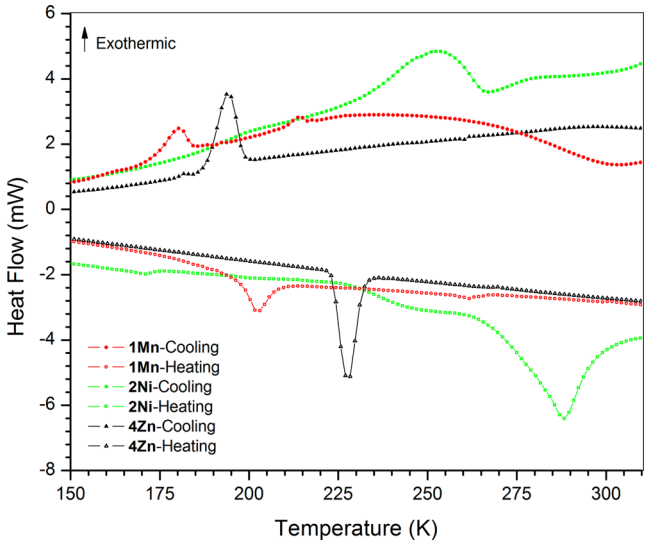

Figure 6. DSC data for compounds **1Mn**, **2Ni**, and **5Zn**.

dx.doi.org/10.1021/ic402200v | *Inorg. Chem.* 2014, 53, 244−256

two exothermal peaks were observed for **1Mn** at 237 K with a relatively small enthalpy of 0.12 kJ mol^{-1}, and at 193 K with a higher enthalpy of 0.54 kJ mol^{-1}, respectively. On heating, both transitions were observed as endothermal peaks at 267 and 202 K respectively.

The highest enthalpy change among all transitions with an enthalpy of 2.51 kJ mol^{-1} was observed in **2Ni**. One sharp exothermal peak centered at 252 K was observed upon cooling and as a sharp endothermal one at 288 K upon heating. The transition of **4Zn** was observed as an exothermal peak with an enthalpy of 1.76 kJ mol^{-1} at 191 K upon cooling and as a sharp endothermal one on heating at 228 K.

Magnetic Properties. The magnetic properties of the three magnetic members **Mn** (S = 5/2), **Ni** (S = 1), and **Cu** (S = 1/2) were investigated using the microcrystalline samples, over the temperature range of 2 K−300 K under different applied fields, H, in units of Tesla. The temperature dependent molar magnetic susceptibility, $\chi_m(T)$, is shown in Figures 7−10 for each compound. The specific heat, $C_p(T, H)$, data for each compound studied here are shown in Figures 8, 9, and 10 and the field dependent magnetization, $M(H)$, is included in the Supporting Information, Figures S4−S9.

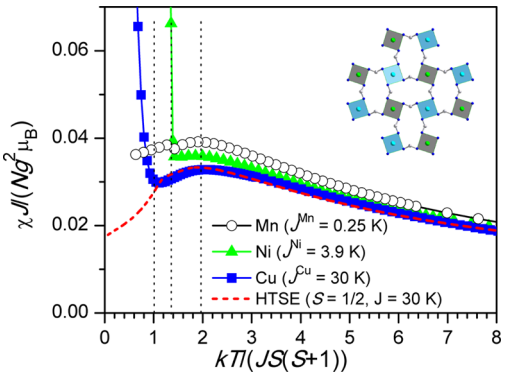

Figure 7. Scaled susceptibilities of the **Mn**, **Ni**, and **Cu** compounds are shown. J refers to the antiferromagnetic coupling constant for the square lattice Heisenberg model $\mathcal{H} = 2J\sum S_i \cdot S_{i+1}$. High-temperature series expansion (HTSE) data according to ref 40 are given for S = 1/2 and J = 30 K for comparison. The black dotted lines are a guide to the eye, see text. The inset shows the connectivity within the plane (square lattice of magnetic ions); for clarity the axial ligands are omitted.

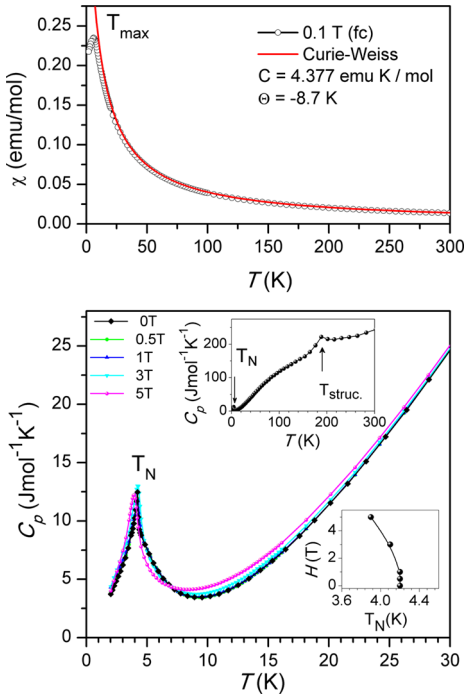

Figure 8. (top panel) Susceptibility measured at 0.1T (fc) and a fit to the Curie−Weiss law for $[Mn(HCOO)_2(HCONH_2)_2]$. The bottom main panel includes the LT range of the specific heat at various fields showing the λ-anomaly related to T_N. The upper *inset* presents the total specific heat up to 300 K with a structural phase transition around 200 K and a magnetic phase transition at 4.2 K. The *inset* (right, bottom) shows the field dependence of the λ-anomaly which indicates antiferromagnetic three-dimensional LRO.

Three compounds (abbreviated **Mn**, **Ni**, **Cu** here without reference to the polymorphs) are representatives of antiferromagnetic Heisenberg square lattices with very similar structural features but different spins. To emphasize the similarities of their physical properties and gain more insight into the underlying model we present the scaled susceptibilities (Figure 7). The high-temperature region is well described by a high-temperature series expansion for the square lattice model.[40,41] $\chi_m(T)$ deviates from a typical Curie−Weiss type of behavior related to the antiferromagnetic exchange, represented by the coupling parameter J between nearest neighbors on the square lattice. We note that all three compounds exhibit a broad maximum $T_{max.}$ = 6.7 K for **Mn**, 28 K for **Ni**, and 58 K for **Cu** associated with the half of the spin entropy released because of short-range order on a square lattice around 2 in units of $kT/(JS(S+1))$. At lower temperatures a sharp upturn in $\chi(T)$ occurs around 1.4 for **Mn** and **Ni** and at 1 for the quantum spin system **Cu** (in units of $kT/(JS(S+1))$). This increase has been frequently associated with the onset of a staggered magnetization at T^*, see for example theoretical and experimental work for the respective spin systems.[41,42]

The development of phenomena such as staggered magnetization in applied fields at nonzero temperatures can be attributed to various origins, such as the staggered orientation of the anisotropy of the g-tensors or spin-canting.[43] The former is associated with the single-ion behavior. Canting may be linked to the equatorial ligands that connect adjacent magnetic centers ($d_{x^2-y^2}$ magnetic orbital) via asymmetric, not coplanar HCOO-bridges. A corrugated square lattice results with adjacent magnetic ions tilted and rotated differently with respect to the crystallographic axis perpendicular to the square lattice (see inset in Figure 7). Additionally, the stacking of these layers is not orthogonal which means that the staggered magnetization of adjacent layers is tilted with respect to the crystallographic axis along the stacking direction.

Furthermore, we note that the development of a staggered magnetization in low-dimensional systems eventually leads to LRO, and a Néel-type of order (T_N) has been discussed for similar systems. However, it is important to stress that experiments carried out for $M(HCOO)_2 \cdot 2H_2O$ and $M(HCOO)_2 \cdot 2$urea which are composed of the same type of square lattice, namely, $M(HCOO)_2$ (4,4) nets and *anti-anti* bridging formate ligands, reveal no significant dependence of T_N upon the interlayer distance.[19,21,44] In detail the following Néel temperatures are reported for $M(HCOO)_2 \cdot 2H_2O$ and $M(HCOO)_2 \cdot 2$urea, respectively: 3.7 and 3.8 K for M = Mn, 15.5 and 15.0 K for M = Ni, 16.8 and 15.5 K for M = Cu.[44] Consequently, it has been concluded that dipolar interactions

dx.doi.org/10.1021/ic402200v | Inorg. Chem. 2014, 53, 244−256

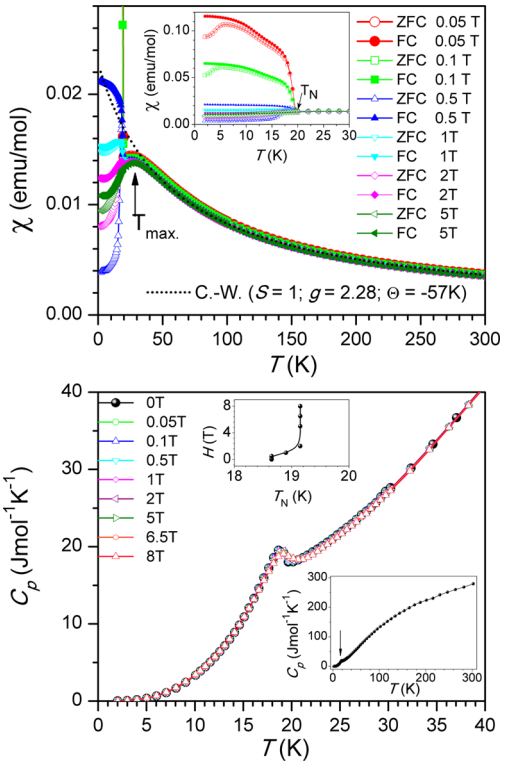

Figure 9. (top panel) Susceptibility measured at various fields and a fit to the Curie–Weiss law for $[Ni(HCOO)_2(HCONH_2)_2]$. The inset gives an enlargement of the LT range showing the significant field dependence below T_N (fc, zfc). The bottom main panel includes the LT range of the specific heat at various fields showing the λ-anomaly related to T_N. The insets depict the total specific heat at zero field up to 300 K (bottom right) and the field dependence of T_N (top middle).

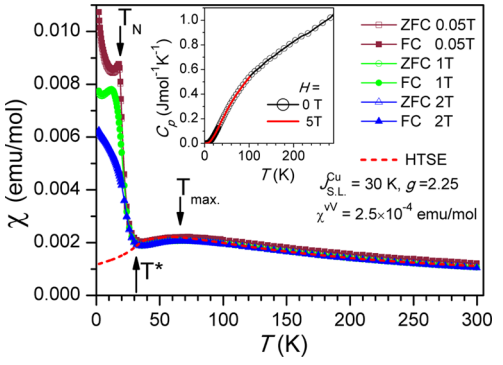

Figure 10. Temperature dependent magnetic susceptibility for $Cu(HCOO)_2(HCONH_2)_2$ measured in different fields in comparison with the HTSE result for the square lattice ($S = 1/2$), see for example reference 40. Marked by arrows: Néel temperature (T_N), T^* onset of the staggered magnetization, and $T_{max.}$ rounded maximum corresponding to the $S = 1/2$ Heisenberg square lattice. The inset gives the total specific heat at zero field and an applied field of 5 T.

between adjacent layers may be neglected, and the interlayer coupling (J^{inter}) would be rather small with $J^{inter}/J \approx 10^{-3}$–$10^{-5}$.

For the series of compounds studied here the occurrence of LRO with $T_N = 4.2$ K for **Mn**, 19.0 K for **Ni**, and 17.5 K for **Cu** (Figures 7–10 and Table 3) is observed and in very good agreement with the reference materials listed above. These phase transitions can be clearly seen in the specific heat data for **Mn** and **Ni** as a λ-type anomaly that appears to be field dependent (Figures 8, 9). Note, that upon increasing applied fields, T_N for the **Mn** compound shifts to lower temperatures in line with antiferromagnetic order, whereas T_N for **Ni** initially increases with the field indicative of ferrimagnetic order. For the **Mn** compound,we estimate the contribution of the anomaly to the total entropy approximately 12% of *Rln*6 and for **Ni** approximately 7% of *Rln*3. However, the measured specific heat of the **Cu** compound (inset Figure 10) does not reveal any evidence attributed to such a LRO, since its magnetic contribution to the total specific heat is expected to be rather small, for example, less than 0.01% of the total entropy *Rln*2, and may be easily overlooked; see also references 45,46.

Table 3. Magnetic Data in K for the $[M(HCOO)_2(HCONH_2)_2]$ Series of Compounds

M	$T_{max.}$	T_N	Θ	J^M
Mn	6.7	4.2	−8.7	0.25
Ni	28	19.0	−57	3.9
Cu	58	17.5	−148	30

The dominating antiferromagnetic character of the magnetic properties is corroborated by the respective field-dependent magnetization measurements (see Supporting Information). In the case of **Cu** one observes at higher temperatures (30 K < $T_{max.}$) a linear increase with applied fields and a rather low magnetization of less than 2.7% at 8 T, which is in line with a significant J^{Cu} parameter of 30 K. Similar coupling constants have been reported for the dihydrate and diurea analogues.[44] Below the onset temperature of the staggered magnetization one observes a steeper increase of $M(H)/M_S$ for applied fields below 1.5 T, which even becomes more pronounced and temperature independent at $T < T_N$. At higher applied fields $M(H)/M_S$ follows a linear response with the same slope for $T \leq 30$ K with the offset of the interpolated intercept $M(0)/M_S$ increasing to 1.5% at 2 K as the temperature is lowered. For the **Mn** compound we observe a slight curvature for $M(H)/M_S$ below 1 T at 2 K and linear field dependence toward higher applied fields. Both magnetization measurements below and above T_N are almost identical which can be understood in terms of the dominant intralayer antiferromagnetic coupling, J^{Mn} of ≈0.25 K, present, well in line with the total value of $M(5T)/M_s$ of only 45%. The **Ni** compound shows similar to the previous ones,a linear field dependence in the region between T_{max} and the onset of a staggered magnetization (T^*): $M(H)/M_S = 10\%$ at 8 T and 25 K, which is in line with $J^{Ni} = 3.9$ K. Below $T_N = 15$ K, here we show the measurements for $T = 2$ K, the weak ferrimagnetic character becomes visible, see Supporting Information. A small hysteresis effect can be seen with a coercivity field $H_c \approx 0.1$ T and remnant magnetization M_R of less than 0.1%. The weak ferrimagnetic behavior is similar in origin to that reported for $Ni(HCOO)_2{\cdot}2H_2O$ and furthermore analyzed in detail by theory.[47]

For all compounds the susceptibility, $\chi(T)$, is field dependent below the onset of the staggered magnetization and decreases with increasing field (Figures 8-10). For **Ni** almost complete suppression becomes visible at $H = 5$ T. The **Cu** compound exhibits a sharp transition at T_N for the lowest field measured. Upon increasing the applied field this feature smears out and shifts to lower temperatures. Both **Mn** and **Cu** display only a slight difference of zero-field cooled versus field cooled susceptibility data, whereas the **Ni** compound reveals a rather pronounced difference in this respect below T_N.

dx.doi.org/10.1021/ic402200v | Inorg. Chem. 2014, 53, 244–256

Further evaluation of the high temperature range (T > 150 K) by fitting the inverse susceptibility to a Curie–Weiss law results in Θ-values of −8.7 K (**Mn**), −57 K (**Ni**), and −148 K (**Cu**), respectively (Table 3, see also Supporting Information). The reciprocal susceptibility for the **Cu** compound is well represented by a HTSE above $T_{max.}$ including a g-value of 2.25 and a small temperature independent van-Vleck type contribution (2.5×10^{-4} emu/mol). The antiferromagnetic intraplanar coupling parameter, J^{Cu} = 30 K, is in excellent agreement with the ones reported for the dihydrate and diurea compounds ($J^{Cu} \approx 33$ K). Thus, it can be concluded that significant interplanar interactions are absent here as well.

For the **Ni** compound an intraplanar coupling constant J^{Ni} = 3.9 K is obtained from scaling the susceptibility and from a molecular field based approach (for details see eqs 10 and 11 in reference 47). The slope of inverse susceptibly (see Supporting Information, Figure S7) is in good agreement with the dominant antiferromagnetic properties of the square lattice in terms of J^{Ni} and T_N. But the overall Θ-value obtained from a Curie–Weiss fit of −57 K is by far too large. From a molecular field approach (see reference 47) one would expect $\Theta^{theo} \approx -20$ K (Curie constant, C = 1.3 emu mol^{-1} K^{-1}) which is very close to $-T_N$, see for comparison the reported values of ≈ −15 K for the dihydrate as well. The difference of $\Delta\Theta = \Theta^* \approx -35$ K in our case is intriguing, and it should be noted that also for the diurea compound a significant larger Θ = −45 K has been observed.[44a] This suggests additional interplanar coupling here and calls for further investigation by neutron and local spectroscopy methods. Above we have reported the LT structure of the **Ni** compound that involves ordering of the axial ligands through simultaneous hydrogen bonding between layers. Likewise one could argue that the hydrogen bonding is similarly effective in the diurea analogue. This scenario would imply that furthermore a crossover into a three-dimensional case occurs and may be related to the additional shift $\Delta\Theta = \Theta^*$ with respect to the inherent properties of the square lattice, see for example references 19 and 44d.

Despite the fact that J^{Mn} = 0.25 K derived from scaling the susceptibility of the **Mn** compound is very small, we find good agreement with the derived $\Theta^{theo.}$ value of −4.3 K ≈ $-T_N$ which is also in excellent agreement with the ones reported for the dihydrate, but again not with our Curie–Weiss fit which indicates Θ = −8.7 K. For the diurea analogue a similar Θ of −8.5 K has been reported. Thus following the same idea as for the **Ni** case we add Θ* = −4.4K to the molecular field based fit, which gives a reasonable agreement with our data, see Supporting Information, Figure S4.

In summary, we have presented the thermodynamic properties of a series of square lattices with S = 1/2, 1, and 5/2. In comparison with dihydrate and diurea analogues and theory, we can conclude that the dominant antiferromagnetic interaction between adjacent magnetic centers is well described by a Heisenberg square lattice model. The conjecture that interplanar interactions can be neglected might be reconsidered because of the peculiarities of significant differences in Θ occurring for those compounds that are considered to undergo a structural order/disorder transition related to hydrogen bonding. However, several aspects are still not well understood or investigated by other methods that likely to shed more light into the intriguing properties of square lattices. In particular, the S = 1/2 case has triggered considerable interest in quantum dynamics worldwide, for example, with recent experimental evidence for phenomena such as entanglement of spins on a square lattice.[48]

IR Spectra. Similar IR spectra but with slight differences were observed for all the five compounds. This is expected given that all the structures have similar bonding environments. Characteristic IR bands of $HCONH_2$ and $HCOO^-$ were observed, and the positions of these bands agree with previous reports for similar compounds (Supporting Information, Table S2, Figure S2).[17,26c,27b,49] The N–H stretching region (3100–3500 cm^{-1}) consist of several IR bands for all the compounds. This could be attributed to the different strengths of the hydrogen bonds formed by the terminating formamide groups.[50] Further, the peak broadening in the same region of **1Mn**, **2Ni**, and **4Zn** indicates that the NH_2 groups are in a disordered environment.[51]

Thermogravimetric Analyses (TGA). Thermogravimetric analyses were performed in air to assess the thermal stabilities of the metal-formato-formamide compounds (Figure 11). All

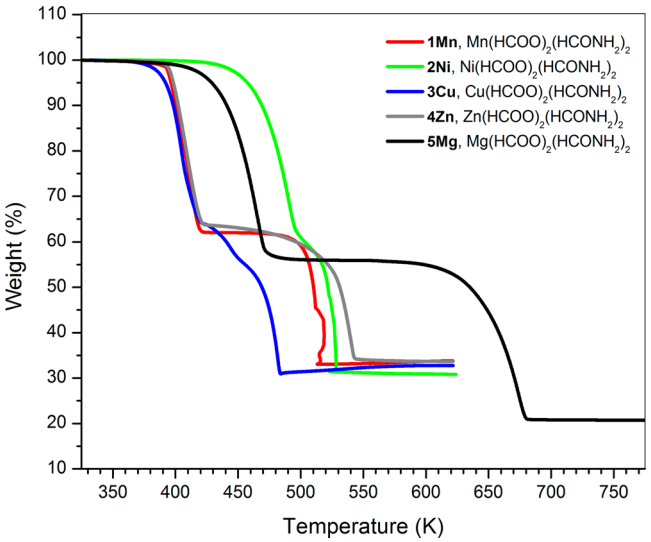

Figure 11. Thermogravimetric analysis data for compounds **1Mn**–**5Mg**.

the compounds were isothermally equilibrated at 323 K followed by a heating to 623 K for **1Mn**–**4Zn** and to 773 K for **5Mg**. No weight loss was observed initially for any of the compounds. This confirmed the absence of guest molecules in the void spaces of the crystal structures. However, the irregularity in the second step of **3Cu** is not well resolved. Similar thermal behavior has been reported for many of the perovskite-like metal formate frameworks with the composition [amineH] [M(HCOO)$_3$].[17,24–27] The two decomposition steps of these formates were assigned as loss of an amine and a formic acid per formula unit followed by a decomposition of metal diformates.

In **1Mn**, the first weight loss occurred at 411 K. The experimental weight loss for the first process is 37.8%. This weight loss corresponds to either a loss of two formamides or two formic acids per formula unit, calculated as 38.3%. Considering the crystal structures of this series and thermal behavior of previously reported formate frameworks, we assume that the terminating formamide ligands are lost in the first step. The resulting phase is presumed to have the stoichiometry of $Mn_3(HCOO)_6$, and it decomposes at 511 K. The experimental residue after complete heating was 33.1% which is in agreement

dx.doi.org/10.1021/ic402200v | Inorg. Chem. 2014, 53, 244–256

with the calculated value of 32.5% based on Mn_3O_4. The nature of the final residue was confirmed by powder X-ray diffraction. In **2Ni**, **3Cu**, **4Zn**, and **5Mg** the first weight losses occurred at 489 K, 400 K, 408 K, and 464 K, respectively. Similar to the **1Mn** compound, these weight losses correspond to loss of terminating formamides in the structures. The experimental and (calculated) percentage weight losses are 37.7 (37.6), 36.2 (36.9), 37.7 (36.7), and 43.9 (44.0), respectively. Further it was observed that the temperatures at which the formamide molecules are lost, parallel the M−O bond strengths of formamide and metal ions and are in the order **2Ni** > **5Mg** > **1Mn** ∼ **4Zn** > **3Cu**.

The resulting phases are presumed to have the stoichiometry of $M(HCOO)_2$. Framework decomposition of **2Ni**−**5Mg** occurred at 524 K, 470 K, 538 K, and 673 K. The final experimental residues were 31.35% for **2Ni**, 33.70% for **4Zn**, and 20.76% for **5Mg**. Calculated values for these residues were 31.28%, 33.15%, and 19.71% based on the final residues of the compounds which were confirmed as NiO, ZnO, and MgO. The experimental residue after the completion of the pyrolysis of **3Cu**, 30.92%, was greater than the value corresponding to the formation of Cu_2O (29.34%) and less than the value corresponding to the formation of Cu_4O_3 (30.99%). This is attributed to the formation of a mixture of Cu_2O and Cu_4O_3 at the end of pyrolysis which was confirmed by the powder XRD pattern of the residue at 493 K (Supporting Information, Figure S3). The slow mass gain of 1.85% after the decomposition of **3Cu** was attributed to the slow oxidation of the residual product to CuO, which was confirmed by the powder XRD of final residue at 623 K. Corresponding weight losses are within the 2% of the calculated values, and the temperatures closely agreed with the thermal decompositions of the reported formate frameworks.

■ ASSOCIATED CONTENT

Supporting Information

X-ray crystallographic information files (CIF) for compounds for **1Mn**, **1bMn**, **1cMn**, **2Ni**, **2bNi**, **3Cu**, **4Zn**, **4bZn**, and **5Mg**, and tables of selected bond lengths and angles and infrared data are available. Magnetization data are provided for compounds **1Mn**, **2Ni**, and **3Cu**. This material is available free of charge via the Internet at http://pubs.acs.org.

■ AUTHOR INFORMATION

Corresponding Authors

*(A.J.J.) E-mail: ajjacob@uh.edu. Phone: 713-743-2785. Fax: 713-743-2787.

*(A.M.) E-mail: amoeller@uh.edu. Phone: 832-842-8846. Fax: 713-743-2709.

Notes

The authors declare no competing financial interest.

■ ACKNOWLEDGMENTS

We thank the R. A. Welch Foundation (#E-0024 and G-099857) for support of this work.

■ REFERENCES

(1) (a) Rao, C. N. R.; Cheetham, A. K.; Thirumurugan, A. *J. Phys.: Condens. Matter* **2008**, *20*, 083202. (b) Cheetham, A. K.; Rao, C. N. R.; Feller, R. K. *Chem. Commun.* **2006**, 4780. (c) Special Issue on Metal-organic Frameworks , Eds: Long, J. R.; Yaghi, O. M.; *Chem. Soc. Rev.* **2009**, *38*, 1213. (d) James, S. L. *Chem. Soc. Rev.* **2003**, *32*, 276. (e) Yaghi, O. M.; O'Keeffe, M.; Ockwig, N. W.; Chae, H. K.; Eddaoudi, M.; Kim, J. *Nature* **2003**, *423*, 705. (f) Yaghi, O. M. *Nat. Mater.* **2007**, *6*, 92. (g) Mueller, U.; Schubert, M.; Teich, F.; Puetter, H.; Schierle-Arndt, K.; Pastre, J. *J. Mater. Chem.* **2006**, *16*, 626. (h) Kitagawa, S.; Kitaura, R.; Noro, S. *Angew. Chem., Int. Ed.* **2004**, *43*, 2334. (i) Férey, G. *Chem. Soc. Rev.* **2008**, *37*, 191.

(2) (a) Furukawa, H.; Ko, N.; Go, Y. B.; Aratani, N.; Choi, S. B.; Choi, E.; Yazaydin, A. O.; Snurr, R. Q.; O'Keeffe, M.; Kim, J.; Yaghi, O. M. *Science* **2010**, *329*, 424. (b) Holst, J. R.; Cooper, A. I. *Adv. Mater.* **2010**, *22*, 5212. (c) Deng, H. X.; Grunder, S.; Cordova, K. E.; Valente, C.; Furukawa, H.; Hmadeh, M.; Gandara, F.; Whalley, A. C.; Liu, Z.; Asahina, S.; Kazumori, H.; O'Keeffe, M.; Terasaki, O.; Stoddart, J. F.; Yaghi, O. M. *Science* **2012**, *336*, 1018. (d) Park, Y. K.; Choi, S. B.; Kim, H.; Kim, K.; Won, B.-H.; Choi, K.; Choi, J.-S.; Ahn, W.-S.; Won, N.; Kim, S.; Jung, D. H.; Choi, S.-H.; Kim, G.-H.; Cha, S.-S.; Jhon, Y. H.; Yang, J. K.; Kim, J. *Angew. Chem., Int. Ed.* **2007**, *46*, 8230.

(3) (a) Rowsell, J. L. C.; Yaghi, O. M. *Angew. Chem., Int. Ed.* **2005**, *44*, 4670. (b) Wu, H.; Zhou, W.; Yildirim, T. *J. Am. Chem. Soc.* **2009**, *131*, 4995. (c) Eddaoudi, M.; Kim, J.; Rosi, N.; Vodak, D.; Wachter, J.; O'Keeffe, M.; Yaghi, O. M. *Science* **2002**, *295*, 469. (d) Wang, X.; Liu, L. M.; Jacobson, A. J. *Angew. Chem., Int. Ed.* **2006**, *45*, 6499.

(4) (a) Pachfule, P.; Das, R.; Poddar, P.; Banerjee, R. *Inorg. Chem.* **2011**, *50*, 3855. (b) Farrusseng, D.; Aguado, S.; Pinel, C. *Angew. Chem., Int. Ed.* **2009**, *48*, 7502. (c) Yoshizawa, M.; Tamura, M.; Fujita, M. *Science* **2006**, *312*, 251. (d) Dang, D. B.; Bai, Y.; He, C.; Wang, J.; Duan, C. Y.; Niu, J. Y. *Inorg. Chem.* **2010**, *49*, 1280.

(5) (a) Allendorf, M. D.; Schwartzberg, A.; Stavila, V.; Talin, A. A. *Chem.—Eur. J.* **2011**, *17*, 11372. (b) Alvaro, M.; Carbonell, E.; Ferrer, B.; Llabrés, I.; Xamena, F. X.; Garcia, H. *Chem.—Eur. J.* **2007**, *13*, 5106. (c) Takaishi, S.; Hosoda, M.; Kajiwara, T.; Miyasaka, H.; Yamashita, M.; Nakanishi, Y.; Kitagawa, Y.; Yamaguchi, K.; Kobayashi, A.; Kitagawa, H. *Inorg. Chem.* **2009**, *48*, 9048. (d) Southon, P. D.; Liu, L.; Fellows, E. A.; Price, D. J.; Halder, G. J.; Chapman, K. W.; Moubaraki, B.; Murray, K. S.; Létard, J. F.; Kepert, C. J. *J. Am. Chem. Soc.* **2009**, *131*, 10998. (e) Halder, G. J.; Kepert, C. J.; Moubaraki, B.; Murray, K. S.; Cashion, J. D. *Science* **2002**, *298*, 1762.

(6) (a) Allendorf, M. D.; Bauer, C. A.; Bhakta, R. K.; Houk, R. J. T. *Chem. Soc. Rev.* **2009**, *38*, 1330. (b) Kent, C. A.; Liu, D.; Meyer, T. J.; Lin, W. *J. Am. Chem. Soc.* **2012**, *134*, 3991. (c) Luo, F.; Batten, S. R. *Dalton Trans.* **2010**, *39*, 4485. (d) Gao, Q.; Wang, X.; Jacobson, A. J. *Inorg. Chem.* **2011**, *50*, 9073.

(7) (a) Kurmoo, M. *Chem. Soc. Rev.* **2009**, *38*, 1353. (b) Special issue on crystal engineering in molecular magnetism: Rovira, C.; Veciana, J. *CrystEngComm* **2009**, *11*, 2031. (c) Molecule-based magnets themed issue: Miller, J. S.; Gatteschi, D. *Chem. Soc. Rev.* **2011**, *40*, 3065. (d) Special issue for the forum on Molecular Magnetism: The Role of Inorganic Chemistry: Coronado, E.; Dunbar, K. R. *Inorg. Chem.* **2009**, *48*, 3293. (e) Huang, Y.-G.; Jiang, F.-L.; Hong, M.-C. *Coord. Chem. Rev.* **2009**, *253*, 2814. (f) Coronado, E.; Espallargas, G. M. *Chem. Soc. Rev.* **2013**, *42*, 1525. (g) Weng, D.; Wang, Z.; Gao, S. *Chem. Soc. Rev.* **2011**, *40*, 3157.

(8) (a) Kuppler, R. J.; Timmons, D. J.; Fang, Q.-R.; Li, J.-R.; Makal, T. A.; Young, M. D.; Yuan, D.; Zhao, D.; Zhuang, W.; Zhou, H.-C. *Coord. Chem. Rev.* **2009**, *253*, 3042. (b) Guo, M.; Cai, H.-L.; Xiong, R.-G. *Inorg. Chem. Commun.* **2010**, *13*, 1590.

(9) (a) Bogani, L.; Vindigni, A.; Sessoli, R.; Gatteschi, D. *J. Mater. Chem.* **2008**, *18*, 4750. (b) Coulon, C.; Clérac, R.; Wernsdorfer, W.; Colin, T.; Miyasaka, H. *Phys. Rev. Lett.* **2009**, *102*, 167204. (c) Coronado, E.; Galán-Mascarós, J. R.; Martí-Gastaldo, C. *J. Am. Chem. Soc.* **2008**, *130*, 14987.

(10) (a) Clemente-León, M.; Coronado, E.; Giménez-López, M. C.; Soriano-Portillo, A.; Waerenborgh, J. C.; Delgado, F. S.; Ruiz-Pérez, C. *Inorg. Chem.* **2008**, *47*, 9111. (b) Liu, Q.; Yu, L.; Wang, Y.; Ji, Y.; Horvat, J.; Cheng, M.; Jia, X.; Wang, G. *Inorg. Chem.* **2013**, *52*, 2817. (c) Wöhlert, S.; Boeckmann, J.; Wriedt, M.; Näther, C. *Angew. Chem., Int. Ed.* **2011**, *50*, 6920.

(11) (a) Shi, P.-F.; Zheng, Y.-Z.; Zhao, X.-Q.; Xiong, G.; Zhao, B.; Wan, F.-F.; Cheng, P. *Chem.—Eur. J.* **2012**, *18*, 15086. (b) Yang, E.-C.; Liu, Z.-Y.; Liu, Z.-Y.; Zhao, L.-N.; Zhao, X.-J. *Dalton. Trans.* **2010**, *39*,

8868. (c) Li, L.; Clarkson, G. J.; Evans, D. J.; Lees, M. R.; Turner, S. S.; Scott, P. *Chem. Commun.* **2011**, *47*, 12646.
(12) (a) Carlin, R. *Magneto-chemistry*; Springer-Verlag: New York, 1985. (b) Itoh, K., Kinoshita, M., Eds.; *Molecular Magnetism: New Magnetic Materials*; Kodansha: Tokyo, Japan, 2000. (b) Whangbo, M.-H.; Koo, H.-J.; Dai, D. *J. Solid State Chem.* **2003**, *176*, 417. (c) Koo, H.-J.; Whangbo, M.-H. *Inorg. Chem.* **2006**, *45*, 4440.
(13) (a) Lapidus, S. H.; Manson, J. L.; Liu, J.; Smith, M. J.; Goddard, P.; Bendix, J.; Topping, C. V.; Singleton, J.; Cortney, D.; Mitchell, J. F.; Schlueter, J. A. *Chem. Commun.* **2013**, *49*, 3558. (b) Landee, C. P.; Turnbull, M. M. *Eur. J. Inorg. Chem.* **2013**, 2266. (c) Manson, J. L.; Carreiro, K. E.; Lapidus, S. H.; Stephens, P. W.; Goddard, P. A.; Del Sesto, R. E.; Bendix, J.; Ghannadzadeh, S.; Franke, I.; Singleton, J.; Lancaster, T.; Möller, J. S.; Baker, P. J.; Pratt, F. L.; Blundell, S. J.; Kang, J.; Lee, C.; Whangbo, M.-H. *Dalton Trans.* **2012**, *41*, 7235. (d) Tanase, S.; Reedijk, J. *Coord. Chem. Rev.* **2006**, *250*, 2501. (e) Cernak, J.; Orendac, M.; Potocnak, I.; Chomic, J.; Orendacova, A.; Skorsepa, J.; Feher, A. *Coord. Chem. Rev.* **2002**, *224*, 51. (f) Mautner, F. A.; Cortes, R.; Lezama, L.; Rojo, T. *Angew. Chem., Int. Ed.* **1996**, *35*, 78. (g) Kabesova, M.; Boca, R.; Melnık, M.; Valigura, D.; Dunaj- Jurco, M. *Coord. Chem. Rev.* **1995**, *140*, 115. (h) McElearney, J. N.; Balagot, L. L.; Muir, J. A.; Spence, R. D. *Phys. Rev. B* **1979**, *19*, 306. (i) Batten, S. R.; Murray, K. S. *Coord. Chem. Rev.* **2003**, *246*, 103.
(14) (a) Osaki, K.; Nakai, Y.; Watanabe, T. *J. Phys. Soc. Jpn.* **1964**, *19*, 717. (b) Krogmann, K.; Mattes, R. *Z. Kristallogr.* **1963**, *118*, 291. (c) Hoy, G. R.; Barros, S.; De, S.; Barros, F.; De, S.; Friedberg, S. A. *J. Appl. Phys.* **1965**, *36*, 936. (d) Takeda, K.; Kawasaki, K. *J. Phys. Soc. Jpn.* **1971**, *31*, 1026. (e) Yamagata, K. *J. Phys. Soc. Jpn.* **1967**, *22*, 582. (f) Pierce, R. D.; Friedberg, S. A. *Phys. Rev. B* **1971**, *3*, 934. (g) Abe, H.; Morigaki, H.; Matsuura, M.; Torii, K.; Yamagata, K. *J. Phys. Soc. Jpn.* **1964**, *19*, 775. (h) Radhkrishna, P.; Gillon, B.; Chevrier, G. *J. Phys.: Condens. Matter* **1993**, *5*, 6447. (i) Kazuko, Z.; Hidenori, H.; Masahiko, T.; Kazuo, Y. *J. Phys. Soc. Jpn.* **2006**, *75*, 104704.
(15) (a) Okada, K. *Phys. Rev. Lett.* **1965**, *15*, 252. (b) Okada, K. *Phys. Rev.* **1967**, *164*, 683. (c) Makita, Y.; Seo, I. *J. Chem. Phys.* **1969**, *51*, 3058. (d) Allen, G. R. *J. Chem. Phys.* **1974**, *60*, 3299. (e) Burger, N.; Fuess, H. *Solid State Commun.* **1980**, *34*, 883. (f) Ishibashi, Y.; Ohya, S.; Takagi, Y. *J. Phys. Soc. Jpn.* **1973**, *34*, 888. (g) Omura, T.; Yoshizumi, K. Y.; Moriyoshi, C.; Itoh, K.; Ikeda, S. *Ferroelectrics* **2003**, *285*, 151.
(16) (a) Wang, X.-Y.; Wang, Z.-M.; Gao, S. *Chem. Commun.* **2008**, 281. (b) Wang, Z.; Hu, K.; Gao, S.; Kobayashi, H. *Adv. Mater.* **2010**, *22*, 1526.
(17) Wang, Z. M.; Zhang, B.; Otsuka, T.; Inoue, K.; Kobayashi, H.; Kurmoo, M. *Dalton Trans.* **2004**, 2209.
(18) Flippen, R. B.; Friedberg, S. A. *J. Chem. Phys.* **1963**, *38*, 2652.
(19) (a) Jørgensen, M. R. V.; Christensen, M.; Schmøkel, M. S.; Iversen, B. B. *Inorg. Chem.* **2011**, *50*, 1441. (b) Okada, K.; Sugie, H. *J. Phys. Soc. Jpn.* **1968**, *25*, 1128. (c) Rønnow, H. M.; McMorrow, D. F.; Harrison, H. *Phys. Rev. Lett.* **1999**, *82*, 3152.
(20) (a) Sapina, F.; Burgos, M.; Escriva, E.; Folgado, J.; Marcos, D.; Beltran, A.; Beltran, D. *Inorg. Chem.* **1993**, *32*, 4337. (b) Viertelhaus, M.; Anson, C. E.; Powell, A. K. *Z. Anorg. Allg. Chem.* **2005**, *631*, 2365. (c) Viertelhaus, M.; Henke, H.; Anson, C. E.; Powell, A. K. *Eur. J. Inorg. Chem.* **2003**, 2283.
(21) (a) Yamagata, K.; Saito, Y.; Abe, T.; Hashimoto, M. *J. Phys. Soc. Jpn.* **1989**, *58*, 3865. (b) Yamagata, K.; Saito, Y.; Abe, T. *J. Phys. Soc. Jpn.* **1989**, *58*, 752. (c) Yamagata, K.; Nojiri, H.; Watamur, S.; Motokawa, M. *J. Phys. Soc. Jpn.* **1991**, *60*, 1140.
(22) (a) Manson, J. L.; Lecher, J. G.; Gu, J.-Y.; Geiser, R.; Schlueter, J. A.; Henning, R.; Wang, X.-P.; Schultz, A. J.; Koo, H. J.; Whangbo, M. H. *Dalton Trans.* **2003**, 2905. (b) Wang, X.; Wei, H.; Wang, Z.; Chen, Z.; Gao, S. *Inorg. Chem.* **2005**, *44*, 572.
(23) (a) Viertelhaus, M.; Adler, P.; Clerac, R.; Anson, C. E.; Powell, A. K. *Eur. J. Inorg. Chem.* **2005**, 692. (b) Calderone, P. J.; Forster, P. M.; Borkowski, L. A.; Teat, S. J.; Feygenson, M.; Aronson, M. C.; Parise, J. B. *Inorg. Chem.* **2011**, *50*, 2159.
(24) (a) Jain, P.; Ramachandran, V.; Clark, R. J.; Zhou, H. D.; Toby, B. H.; Dalal, N. S.; Kroto, H. W.; Cheetham, A. K. *J. Am. Chem. Soc.* **2009**, *131*, 13625. (b) Jain, P.; Dalal, N. S.; Toby, B. H.; Kroto, H. W.; Cheetham, A. K. *J. Am. Chem. Soc.* **2008**, *130*, 10450. (c) Sánchez-Andújar, M.; Presedo, S.; Yáñez-Vilar, S.; Castro-García, S.; Shamir, J.; Señarís-Rodríguez, M. A. *Inorg. Chem.* **2010**, *49*, 1510. (d) Wang, X. Y.; Gan, L.; Zhang, S. W.; Gao, S. *Inorg. Chem.* **2004**, *43*, 4615.
(25) (a) Cheong, S.-W.; Mostovoy, M. *Nat. Mater.* **2007**, *6*, 13. (b) Rogez, G.; Viart, N.; Drillon, M. *Angew. Chem., Int. Ed.* **2010**, *49*, 1921.
(26) (a) Xu, G.-C.; Ma, X.-M.; Zhang, L.; Wang, Z.-M.; Gao, S. *J. Am. Chem. Soc.* **2010**, *132*, 9588. (b) Xu, G.-C.; Zhang, W.; Ma, X.-M.; Chen, Y.-H.; Zhang, L.; Cai, H.-L.; Wang, Z.-M.; Xiong, R.-G.; Gao, S. *J. Am. Chem. Soc.* **2011**, *133*, 14948. (c) Wang, Z. M.; Zhang, B.; Inoue, K.; Fujiwara, H.; Otsuka, T.; Kobayashi, H.; Kurmoo, M. *Inorg. Chem.* **2007**, *46*, 437.
(27) (a) Stroppa, A.; Jain, P.; Barone, P.; Marsman, M.; Perez-Mato, J. M.; Cheetham, A. K.; Kroto, H. W.; Picozzi, S. *Angew. Chem., Int. Ed.* **2011**, *50*, 5847. (b) Hu, K.-L.; Kurmoo, M.; Wang, Z.-M.; Gao, S. *Chem.—Eur. J.* **2009**, *15*, 12050.
(28) (a) Shang, R.; Sun, X.; Wang, Z.-M.; Gao, S. *Chem.—Asian. J.* **2012**, *7*, 1697. (b) Fu, D.-W.; Zhang, W.; Cai, H.-L.; Zhang, Y.; Ge, J.-Z.; Xiong, R.-G.; Huang, S. D.; Nakamura, T. *Angew. Chem., Int. Ed.* **2011**, *50*, 11947. (c) Liu, B.; Shang, R.; Hu, K.; Wang, Z.; Gao, S. *Inorg. Chem.* **2012**, *51*, 13363.
(29) (a) Pato-Doldán, B.; Sánchez-Andújar, M.; Gómez-Aguirre, L. C.; Yáñez-Vilar, S.; López-Beceiro, J.; Gracia-Fernández, C.; Haghighirad, A. A.; Ritter, F.; Castro-García, S.; Señarís-Rodríguez, M. A. *Phys. Chem. Chem. Phys.* **2012**, *14*, 8498. (b) Rossin, A.; Ienco, A.; Costantino, F.; Montini, T.; Credico, B. D.; Caporali, M.; Gonsalvi, L.; Fornasiero, P.; Peruzzini, M. *Cryst. Growth Des.* **2008**, *8*, 3302. (c) Zhou, B.; Imai, Y.; Kobayashi, A.; Wang, Z.-M.; Kobayashi, H. *Angew. Chem., Int. Ed.* **2010**, *50*, 11441. (d) Imai, Y.; Zhou, B.; Ito, Y.; Kobayashi, A.; Wang, Z.-M.; Kobayashi, H. *Chem.—Asian J.* **2012**, *7*, 2786.
(30) (a) Slater, J. C. *J. Chem. Phys.* **1941**, *9*, 16. (b) Banerjee, S.; Nath, D.; Chaudhuri, B. K. *Phys. Rev. B* **1981**, *24*, 6469.
(31) (a) Rettig, S. J.; Thompson, R. C.; Trotte, J.; Xia, S. *Inorg. Chem.* **1999**, *38*, 1360. (b) Sengupta, O.; Song, Y.; Mukherjee, P. S. *Dalton Trans.* **2009**, 10343. (c) S. Fortier, S.; Creber, K. A. M. *Acta Crystallogr.* **1985**, *C41*, 1763.
(32) *APEX2 User Manual*, Version 1.27; Bruker AXS Inc.: Madison, WI, 2005.
(33) Sheldrick, G. M. *SHELXS97, Program for Crystal Structure Resolution*; University of Göttingen: Göttingen, Germany, 1997.
(34) Sheldrick, G. M. *SHELXS97, Program for Crystal Structure Analysis*; University of Göttingen: Göttingen, Germany, 1997.
(35) Farrugia, L. *J. Appl. Crystallogr.* **1999**, *32*, 837.
(36) Sheldrick, G. M. *CELL_NOW*; Bruker AXS: Madison, WI, 2002.
(37) Bain, G. A.; Berry, J. F. *J. Chem. Educ.* **2008**, *85*, 532.
(38) (a) Hine, J.; King, R. S. M.; Midden, W. R.; Sinha, A. *J. Org. Chem.* **1981**, *46*, 3186. (b) Brown, R. S.; Bennet, A. J.; Slebocka-Tilk, H. *Acc. Chem. Res.* **1992**, *25*, 481. (c) Kallies, B.; Mitzner, R. *J. Mol. Model.* **1998**, *4*, 183. (d) Krug, J. P.; Popelier, P. L. A.; Bader, R. F. W. *J. Phys. Chem.* **1992**, *96*, 7604. (e) Almerindo, G. I.; Pliego, J. R. *J. Braz. Chem. Soc* **2007**, *18*, 469. (f) Slebocka-Tilk, H.; Sauriol, F.; Monette, M.; Brown, R. S. *Can. J. Chem.* **2002**, *80*, 1343. (g) Gorb, L.; Asensio, A.; Tuñón, I.; Ruiz-López, M. F. *Chem.—Eur. J.* **2005**, *11*, 6743. (h) Pliego, J. R. *Chem. Phys.* **2004**, *306*, 273. (i) Cascella, M.; Raugei, S.; Carloni, P. *J. Phys. Chem. B* **2004**, *108*, 369.
(39) Chulkevich, A. K.; Lavrent'ev, I. P.; Moravskii, A. P.; Khidekel', M. L.; Ponomarev, V. I.; Filipenko, O. S.; Atovmyan, L. O. *Koord. Khim.* **1986**, *12*, 470; *Coord. Chem. (Engl. Trans)* **1986**, 285.
(40) Takahashi, M. *Phys. Rev. B* **1989**, *40*, 2494.
(41) (a) Stanley, H. E. *Phys. Rev B* **1967**, *40*, 1546. (b) Carlin, L.; van Duyneveldt, A. J. *Magnetic Properties of Transition Metal Complexes*; Springer-Verlag: New York, 1977.
(42) Cuccoli, A.; Tognetti, V.; Verrucchi, P.; Vaia, R. *Phys. Rev. B* **1998**, *58*, 14151.

(43) (a) Koyama, K.; Nobumasa, H.; Matsuura, M. *J. Phys. Soc. Jpn.* **1987**, *56*, 1553. (b) Koyama, K.; Matsuura, M. *J. Phys. Soc. Jpn.* **1985**, *54*, 4085. (c) Kahn, O. *Molecular Magnetism*; Wiley-VCH: New York, 1993.
(44) (a) Yamagata, K.; Abe, T.; Higuchi, Y.; Deguchi, H.; Takeda, K.; Kaneko, K.; Nojiri, H.; Motokawa, M. *J. Magn. Magn. Mater.* **1992**, *104*, 803. (b) Yamamoto, Y.; Matsuura, M.; Haseda, T. *J. Phys. Soc. Jpn.* **1976**, *40*, 1300. (c) Yamagata, K.; Kozuka, Y.; Morita, T. *J. Phys. Soc. Jpn.* **1981**, *50*, 421. (d) Clarke, S.; Harrison, A.; Mason, T. E.; McIntyre, G. J.; Visser, D. *J. Phys.: Condens. Matter* **1992**, *4*, L71.
(45) Matsuura, M.; Takeda, K.; Satoh, T.; Sawada, Y.; Machado da Silva, J. M. *Solid State Commun.* **1973**, *13*, 467.
(46) Sengupta, P.; Sandvik, A. W.; Singh, R. R. P. *Phys. Rev. B* **2003**, *68*, 094423.
(47) Kageyama, H.; Khomskii, D. I.; Levitin, R. Z.; Vasil'ev, A. N. *Phys. Rev. B* **2003**, *67*, 224422.
(48) Christensen, N. B.; Rønnow, H. M.; McMorrow, D. F.; Harrison, A.; Perring, T. G.; Enderle, M.; Coldea, R.; Regnault, L. P.; Aeppli, G. *Proc. Natl. Acad. Sci. U.S.A.* **2007**, *104*, 15264.
(49) McNaughton, D.; Evans, C. J.; Lane, S.; Nielsen, C. J. *J. Mol. Spectrosc.* **1999**, *193*, 104.
(50) Williams, D. H.; Fleming, I. *Spectroscopic Methods in Organic Chemistry*, 5th ed.; McGraw-Hill: Beijing, China, 1998.
(51) (a) Larkin, P. *Infrared and Raman Spectroscopy; Principles and Spectral Interpretation*; Elsevier: New York, 2011. (b) Naïli, H.; Mhiri, T.; Daoud, A. *Int. J. Inorg. Mater.* **2001**, 393.